

A spectroscopic investigation of the afterglow and recombination process in a microsecond pulsed glow discharge

Xiaomei Yan,^a Yiming Lin,^b Rongfu Huang,^b Wei Hang^{*b} and Willard W. Harrison^c

Received 25th June 2009, Accepted 21st December 2009

First published as an Advance Article on the web 14th January 2010

DOI: 10.1039/b912558b

The emission characteristics of afterglow in a microsecond pulsed glow discharge atomic source are studied to obtain insight into the excitation and recombination processes of analytes and fill gases. Each emission line features an initial intense peak at the beginning of the discharge pulse. The afterglow, which has been observed in the temporal behavior for some emission temporal profiles of analytes and discharge gases, exhibits an intense post-pulse signal maximized at 25–35 μs after plasma termination, with a broader profile than their initial peaks. The afterglow of Ar I and Cu I spectra last approximately 100 μs and 300 μs , respectively, after the argon discharge pulse at 2.0 torr pressure. The intensity of the afterpeak increases with the pulse width between 2 μs to 200 μs . A study of fourteen Ar I and twenty-seven Cu I lines show that transitions from high energy levels (5p [14.5–14.7 eV] for Ar and above 6 eV for Cu) are relatively stronger in the afterglow. The highly excited argon and copper atoms are thought to be generated *via* the recombination of ions and electrons. The results are explained primarily in terms of an electron-electron-ion three-body recombination process.

Introduction

The glow discharge (GD) has received wide acceptance and increasing interest as a means of direct solid sample spectrochemical analysis,^{1–3} which in turn has led to increased plasma diagnostics and modeling studies.^{4–10} A better understanding of the fundamental processes in the glow discharge is desirable for optimal operation and instrumentation development. In the vast majority of GD used, the plasma is generated in a continuous direct current (dc) mode. However, advantages have resulted from pulsed glow discharges in the microsecond range serving as an ion source for a time-of-flight mass spectrometer (TOFMS),^{11–13} which brings a breakthrough in the field of thin film analysis¹⁴ and also the ability for obtaining either atomic, molecular or structural information.¹⁵ Optical emission also benefits from pulsed mode GD operation,¹⁶ and compared with the lengthy mass transport process in mass spectrometry, the immediacy of optical measurement offers advantages for plasma process evaluation. The millisecond pulsed GD maintains a quasi-stationary or steady state,^{17–19} but the microsecond pulse technique offers more appropriate time resolution for acquiring information of the physical processes in the glow discharge.

Generally, recombination processes are thought to account for the afterglow of a decay plasma.²⁰ Ohebsian *et al.*²¹ found the excited levels of the titanium atom are principally populated by electron-ion recombination processes in the afterglow of a 100 μs Ti–Ar hollow cathode discharge in the pressure range 0.1 to 5 torr. The recombination of free electrons with positive ions has

been the subject of numerous theoretical and experimental investigations.^{22–24} The loss of electrons either through ambipolar diffusion or through recombination in an afterglow can be measured accurately in a high plasma density by observing the change of the resonant wavelength of a microwave cavity enclosing the discharge container.²² Studies in the helium, neon, argon, hydrogen, nitrogen, and oxygen electrodeless discharge afterglow indicated that the radiative recombination coefficient is in the range 10^{-8} – 10^{-6} $\text{cm}^3 \text{s}^{-1}$ for pressure varied from 2 to 30 torr.²² Of the several possible recombination processes for rare gases, dissociative recombination has been most frequently applied to explain the large discrepancies (several orders of magnitude) between experimental recombination coefficients and the theoretical values (10^{-12} $\text{cm}^3 \text{s}^{-1}$) based on the radiative recombination theory.^{8,25,26} From spectral line-shape (Doppler effect) studies in a magnetron generated neon pulse afterglow at the pressure of tens of torr, Connor and Biondi concluded²⁷ that dissociative recombination, $\text{Ne}_2^+ + e \rightarrow (\text{Ne}_2^*)_{\text{unstable}} \rightarrow \text{Ne}^* + \text{Ne}$, is the process responsible for the population of the excited neon levels and also for the large electron loss in neon afterglow. In the early 1960's, a three-body recombination mechanism was proposed to account for the large coefficient values at rather high electron and ion densities ($n_e > 10^{12}$ cm^{-3}).^{28,29} The three-body recombination, also called collisional-radiative recombination, involves one ion and two electrons, in which an electron, as a result of a collision with another electron, loses enough energy to be captured in one of the excited electronic orbits of an ion, followed by radiative transition or superelastic collisions with electrons to a lower level, finally ending in a ground state.^{20,29} The recombination coefficient (around 10^{-10} $\text{cm}^3 \text{s}^{-1}$) of the electron-electron-ion three-body recombination process has been measured and calculated as a function of electron temperature and density for a milli-torr pressure range 1 ms duration magnetically confined helium and hydrogen plasma.³⁰ The

^aKey Laboratory for Chemical Biology of Fujian Province, College of Chemistry and Chemical Engineering, Xiamen University, China

^bKey Laboratory of Analytical Science of Xiamen University, College of Chemistry and Chemical Engineering, Xiamen University, China

^cDepartment of Chemistry, University of Florida, Gainesville, FL, 32611, USA

afterglow study was further motivated by gas-laser energy transfer investigations,^{21,31–33} since noble gases are frequently used as an active medium for the formation of the population inversion. Collisional-radiative recombination was shown to be the fundamental excitation process of the He atom in the afterglow of a low pressure (1.6 torr) glow discharge.³¹

For the millisecond pulsed GD-MS study, King *et al.*^{34,35} suggested that argon ion-electron recombination dominates metastable formation during the afterglow. For both argon and copper analyst emission, transitions from high-energy electronic states predominate during the afterpeak time regime. Bogaerts *et al.*⁹ developed a modeling network to describe the behavior of the various plasma species and suggested that the afterpeak was attributed to collisional-radiative recombination. In a later paper, this suggestion was attenuated and the dominant process of dissociative-recombination for ms-pulsed discharges was suggested,⁸ because collisional-radiative recombination could only be dominant if the electron and ion densities would rise by two orders of magnitude in the afterglow, which was not observed by Gamez *et al.*³⁶ Harrison and coworkers¹⁹ observed that the analyte (sputtered) ion signals increased to a maximum approximately 0.5 ms after the discharge power was terminated, while signals for support gas and polyatomic ions exhibited no such enhancement. This behavior was attributed to an increase in Penning ionization of analyte atoms due to an increase in argon metastable density just after the power cessation. The authors suggested that the increase in the metastable density could be due to enhanced argon ion-electron recombination, producing highly excited argon atoms, many of which then radiatively relax into the metastable levels.¹⁸ Studies by Human and his colleagues⁶ with a 4 ms pulsed dc Grimm-type lamp revealed that argon metastable absorption increases to a maximum approximately 100–150 μ s after termination of the current. Recombination was thought to be the dominant process during the afterglow, and the increase in cathode metal emission is the result of excitation by high energy electrons created by collisions of pairs of metastable atoms, when one of the partners is ionized and the other decays to the ground state.

Typically, the ion and electron densities are $10^{10}\sim 10^{12}$ cm^{-3} in millisecond pulsed discharge.^{9,36} However, in microsecond pulsed glow discharge, the electron and ion densities are higher, *i.e.*, in the order of $10^{13}\sim 10^{14}$ cm^{-3} .^{10,37} Hence, it is well possible that other recombination processes are important in microsecond pulsed GD than that in the millisecond-pulsed discharge. Thus, the recombination process in gas discharges has received much attention and is of considerable interest to explain the excitation processes during the afterglow in the present paper. From our studies of a microsecond pulsed GD, we believe the emission temporal profiles of argon and sputtered copper atoms and their population processes suggest a three-body recombination as a dominant process of the afterglow plasma decay. Reported here is the study of the atomic excitation and recombination processes in the μ s-pulsed GD plasma, with main emphasis on the afterglow or post-pulse region. The afterglow exhibits an intense post-pulse signal maximum (known as afterpeak) at 25–30 μ s after the voltage pulse termination, with a broader time profile than the initial peak, reflecting the different dominant excitation mechanisms during the pulse *vs.* afterglow regions.

Experimental

The experimental apparatus has been described fully elsewhere³⁸ and therefore only a brief description will be presented here. The glow discharge cell was a six-way cross with 2.75" flanges equipped with 4 quartz windows. Samples were prepared by pressing copper powder (Johnson Matthey Inc.; 99.5% pure) into a disc. The copper disc (4.5 mm diameter and 1 mm thickness) was mounted onto a direct insertion probe. Ultrahigh-purity argon (Alfagaz, Walnut Creek, CA, 99.9995% pure) served as the plasma gas. A high voltage pulse generator (Model 350, Velonex, Santa Clara, CA, USA) was used to pulse the glow discharge in the microsecond regime.

The time-resolved emission signals, giving the population of the excited levels, were measured with a Spex 1680B monochromator (0.2 nm resolution, 50 μ m slit) equipped with a Hamamatsu R955 photomultiplier. The PMT output was amplified and then fed into a 500 MHz digital storage oscilloscope (Hewlett Packet 54542C Digitizing Oscilloscope, 2 Gsa/s), which was set to average the signal continuously over 128 successive cycles of the discharge. The leading edge of the applied voltage synchronized the signal profiles. The GD pressure was kept constant at 2.0 torr argon pressure except later in Fig. 4, where 2.4 torr was used. The discharge duration was varied from 2 to 200 μ s, and pulse repetition rate was 50 Hz. The peak discharge current was about 70 mA with pulse magnitude of 2 kV. The average power depositing in the plasma was less than 2 watts for 200 μ s pulse, but the instantaneous power reached 140 W. Since all transitions to the ground states of Ar I are in the vacuum ultraviolet region, the transitions from 5p or 4p \rightarrow 4s (the 1s₅ and 1s₃ metastable species together with the 1s₂ and 1s₄ resonant species) were used to study Ar I. The excitation of the copper neutrals was studied by monitoring twenty-seven Cu I transitions in the wavelength range 200–600 nm.

Afterglow processes

During the time immediately after removal of the GD applied voltage, various volume and wall processes contribute to the diminishment, and sometimes replenishment, of populations of electrons, ions, excited species, and neutrals. The variation of electron density during this post-pulse period is, in general, the result of a number of competing processes: ambipolar diffusion with subsequent neutralization by an incident positive ion at the walls, electron-ion recombination, and attachment of electrons to the atoms or molecules. Usually the attachment coefficient is negligible, and diffusion is only important at low pressures (below 1 torr) and the characteristic diffusion length is small.^{20,39} If the three-body recombination process mainly accounts for the electron loss during the afterglow, and assuming that the concentrations of positive ions and electrons are equal, it follows:

$$\frac{1}{n_e^2} - \frac{1}{n_{e0}^2} = 2\alpha_e t \quad (1)$$

where n_e represents the electron density, n_{e0} is the electron density at time $t = 0$, α_e is the recombination coefficient, and a plot of $1/n_e^2$ *vs.* t should result in a straight line. If the electrons disappear due to ambipolar diffusion, then

$$n_e = n_{e0} \exp(-t/\tau) \quad (2)$$

where τ is the characteristic decay time, related to the ambipolar diffusion coefficient D_a by $\tau = A^2/D_a$. A is the characteristic diffusion length of the container. In eqn (2), the plot of $\log n_e$ vs t should be a straight line, which gives a method of distinguishing experimentally between the two processes.

The deduction of the α_e or D_a coefficient from experimental electron density decay data which fits Eqn 1 or 2 over a sufficient range of electron densities can provide the most direct determination of electron-ion recombination rate or ambipolar diffusion coefficient. If the gas pressure is sufficiently high, e.g. 15–30 torr in Ref. 22, the diffusion loss of the electrons and ions to the walls of the container will be small compared to the loss by volume recombination. Langmuir probe²⁴ or microwave^{23,40} techniques have been used to measure the decay of electron density from an initially ionized gas. The probe measurement requires that the mean free path greatly exceeds the probe dimension, so it is essential that the gas pressure should be below about 1 torr. Thus, the probe measurements have been subject to criticisms.²⁰ By contrast, the microwave permittivity measurement can be used in afterglows at the pressure one order of magnitude greater at least compared with the probe measurement. The electron density is determined by the shift of the resonant frequency of the cavity in which the discharge occurs, therefore more accurate results can be given for a dense plasma.

Electron density measurement in a continuous dc GD has been reported by several authors, and it was found to vary with discharge type, source structure, and operating conditions. A value of ca. 10^{14} cm^{-3} was derived from the line profiles of He 447.1 nm and Ar 415.8 nm for a moderate current (40–80 mA) Grimm-type argon GD at a pressure range of 2–11 torr.⁴¹ Meanwhile, electron densities were found on the order of 10^{11} cm^{-3} in a 10 mA, 2–3 torr dc GD by Fang using Langmuir probe measurements.⁴² In the microsecond pulsed GD for this experiment, much higher instantaneous voltage was applied to the cathode, resulting in an intense transient current of 70 mA, so many more electrons should be generated during the pulse-on period. Electron density measurements in the transient afterglow of a microsecond pulsed discharge present significant experimental problems; however, it can be estimated roughly from the current and pulse duration. For example, a 70 mA current lasting 10 μs will generate 4.4×10^{12} electrons. The average life time of electrons is about 50–100 μs at several torr environment deduced from the data in Ref. 43. If those electrons reside in a 1 cm^3 space evenly, the electron density is $4.4 \times 10^{12} \text{ cm}^{-3}$. However, electrons show the highest density at the narrow negative glow zone, which usually is the observation spot for emission,⁴⁴ the density is at least one order of magnitude higher than the average number. Higher density can be achieved with longer pulse width, but pulse width exceeding the life time of electron should not further increase the electron density significantly. Therefore, in our experiment, electron density in the observation spot should be about 10^{13} – 10^{14} cm^{-3} , which is in accord with Ref. 10 and 37.

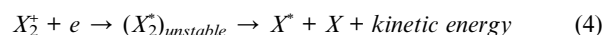
In this study, the observation of intense afterglow radiation (extending to 100 μs for a 10 μs pulse, or 300 μs for a 200 μs pulse) was taken as an evidence for the dominance of the recombination process. It could be argued that the afterglow radiation might

have occurred as a result of electrons diffusing to the wall. However, the above process could not contribute to the afterglow emission in our instrumental setup, since the radiation measurement was carried out in an axial direction, where the distance between the cathode surface and quartz window is about 10 cm.

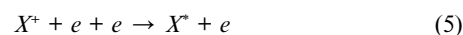
The three most often considered recombination processes occurring in a rare gas afterglow are listed as follows: radiative recombination^{22,45}



dissociative recombination^{8,46,47}



and three-body recombination with an electron as its third body^{9,30,48}



Radiative recombination was usually considered to be negligible in a dense ($n_e > 10^{12} \text{ cm}^{-3}$) plasma, since a calculation from theory can not explain the large recombination coefficient measured.^{8,9} As described in eqn (4), dissociative recombination involves non-radiative capture of an electron by a molecular ion, followed by dissociation into two neutral fragments, one of which is in an excited electronic state. Dissociative recombination can only occur if molecular ions are present in the discharge. The TOFMS measurement during the afterglow of a microsecond pulsed GD indicated that the ion signal of both the argon dimers and copper dimers are much lower (less than 1%) than their single charged ions.¹¹ Also there are no characteristic spectral lines reported so far that can prove the existence of abundant dimers of rare gases or analytes in a pulsed microsecond GD plasma. Moreover, as estimated above, the electron density in the experiment should be about 10^{13} – 10^{14} cm^{-3} . In Ref. 8, the rate coefficient of electron-ion three-body recombination is equal to $10^{-19} (T_e/300)^{-9/2} \text{ cm}^6 \text{ s}^{-1}$, whereas the rate coefficient of dissociative recombination is $8.5 \times 10^{-7} (T_e/300)^{-0.67} (T_g/300)^{-0.58} \text{ cm}^3 \text{ s}^{-1}$. Based on electron and ion densities of 10^{13} – 10^{14} cm^{-3} and $T_e = T_g = 300 \text{ K}$, the rate of electron-ion three-body recombination is calculated to be 10^{20} – 10^{23} s^{-1} in the afterglow, and the rate of dissociative recombination is only 10^{18} – 10^{20} s^{-1} , if the Ar_2^+ concentration is 1% of the Ar^+ concentration. Therefore, the dissociative recombination process should not be the dominant recombination process in the afterglow of microsecond analytical glow discharge. Consequently, the remaining process described in eqn (5) should be the most likely candidate to account for the intense afterglow phenomena. Note that these estimates are different for millisecond pulsed discharges, where the electron and ion densities are typically lower, i.e., in the order of 10^{10} – 10^{12} cm^{-3} ,^{8,9} and the rate of dissociative recombination was calculated to be higher than the three-body recombination rate.⁸

Results and discussion

We have monitored the temporal behavior of numerous lines emitted from the excited levels of Ar and Cu in a microsecond

pulsed glow discharge operated at 2.0 kV and 2.0 torr argon pressure with both 10 μs and 200 μs pulse widths. Detailed information about these neutral transitions was tabulated in Table 1 and 2 for Ar and Cu, respectively. The partial energy level diagrams for argon and copper are displayed in Fig. 1(a) and (b), respectively.^{49,50} The observed time variation of emission signal indicates the mechanisms responsible for the population of these levels during the discharge pulse and the afterglow.

Table 1 Monitored Ar I transitions at microsecond-pulsed glow discharge conditions

No.	Transition	Wavelength/nm	E_k (cm^{-1})	E_i (cm^{-1})
1	3p9–5p[5/2] \rightarrow 1s5–4s[3/2]	420.1	116943	93144
2	3p8–5p[5/2] \rightarrow 1s5–4s[3/2]	419.1	116999	93144
	3p4–5p'[3/2] \rightarrow 1s3–4s'[1/2]	419.1	118407	94554
3	3p6–5p[3/2] \rightarrow 1s5–4s[3/2]	415.9	117184	93144
4	3p6–5p[3/2] \rightarrow 1s4–4s[3/2]	426.6	117184	93751
5	3p1–5p'[1/2] \rightarrow 1s2–4s'[1/2]	425.9	118871	95400
6	2p8–4p[5/2] \rightarrow 1s5–4s[3/2]	801.5	105617	93144
7	2p7–4p[3/2] \rightarrow 1s5–4s[3/2]	772.4	106087	93144
8	2p6–4p[3/2] \rightarrow 1s5–4s[3/2]	763.5	106238	93144
9	2p4–4p'[3/2] \rightarrow 1s5–4s[3/2]	714.7	107132	93144
10	2p3–4p'[3/2] \rightarrow 1s5–4s[3/2]	706.7	107290	93144
11	2p2–4p'[1/2] \rightarrow 1s5–4s[3/2]	696.5	107496	93144
12	2p5–4p[1/2] \rightarrow 1s4–4s[3/2]	751.5	107054	93751
13	2p2–4p'[1/2] \rightarrow 1s3–4s'[1/2]	772.4	107496	94544
14	2p1–4p'[1/2] \rightarrow 1s2–4s'[1/2]	750.4	108723	95400

Table 2 Monitored Cu I transitions at microsecond-pulsed glow discharge conditions.^a

No.	Transition	Wavelength/ nm	E_k / cm^{-1}	E_i / cm^{-1}
1	4p'' $^2\text{D}_{5/2} \rightarrow 4s^2 \text{ } ^2\text{D}_{5/2}$	220.0	56651	11203
2	4p'' $^2\text{P}_{3/2} \rightarrow 4s^2 \text{ } ^2\text{D}_{5/2}$	221.5	56344	11203
3	5p $^2\text{P}_{3/2} \rightarrow 4s^2 \text{ } ^2\text{D}_{5/2}$	261.8	49383	11203
4	5p $^2\text{P}_{1/2} \rightarrow 4s^2 \text{ } ^2\text{D}_{3/2}$	276.6	49383	13245
5	5d $^2\text{D}_{3/2} \rightarrow 4p \text{ } ^2\text{P}_{1/2}$	402.3	55388	30535
6	4d $^2\text{D}_{3/2} \rightarrow 4p \text{ } ^2\text{P}_{1/2}$	515.3	49935	30535
7	5d $^2\text{D}_{5/2} \rightarrow 4p \text{ } ^2\text{P}_{3/2}$	406.3	55391	30784
8	4d $^2\text{D}_{5/2} \rightarrow 4p \text{ } ^2\text{P}_{3/2}$	521.8	49942	30784
9	4p $^2\text{P}_{1/2} \rightarrow 4s \text{ } ^2\text{S}_{1/2}$	327.4	30535	0
10	4p $^2\text{P}_{3/2} \rightarrow 4s \text{ } ^2\text{S}_{1/2}$	324.8	30784	0
11	4p' $^4\text{P}_{3/2} \rightarrow 4s \text{ } ^2\text{S}_{1/2}$	249.2	40114	0
12	4p' $^4\text{D}_{3/2} \rightarrow 4s \text{ } ^2\text{S}_{1/2}$	224.4	44544	0
13	4p' $^2\text{P}_{1/2} \rightarrow 4s \text{ } ^2\text{S}_{1/2}$	218.2	45821	0
14	4p' $^2\text{P}_{3/2} \rightarrow 4s \text{ } ^2\text{S}_{1/2}$	217.8	45879	0
15	4p' $^2\text{D}_{3/2} \rightarrow 4s \text{ } ^2\text{S}_{1/2}$	216.5	46173	0
16	4p $^2\text{P}_{3/2} \rightarrow 4s \text{ } ^2\text{D}_{5/2}$	510.6	30784	11203
17	4p' $^4\text{F}_{7/2} \rightarrow 4s \text{ } ^2\text{D}_{5/2}$	333.8	41153	11203
18	4p' $^4\text{D}_{7/2} \rightarrow 4s \text{ } ^2\text{D}_{5/2}$	309.4	43514	11203
19	4p' $^4\text{D}_{5/2} \rightarrow 4s \text{ } ^2\text{D}_{5/2}$	301.1	44406	11203
20	4p' $^2\text{F}_{7/2} \rightarrow 4s \text{ } ^2\text{D}_{5/2}$	296.1	44963	11203
21	4p' $^2\text{D}_{5/2} \rightarrow 4s \text{ } ^2\text{D}_{5/2}$	282.4	46598	11203
22	4p $^2\text{P}_{1/2} \rightarrow 4s \text{ } ^2\text{D}_{3/2}$	578.2	30535	13245
23	4p' $^4\text{F}_{5/2} \rightarrow 4s \text{ } ^2\text{D}_{3/2}$	353.0	41563	13245
24	4p' $^2\text{F}_{5/2} \rightarrow 4s \text{ } ^2\text{D}_{3/2}$	328.0	43726	13245
25	4p' $^4\text{D}_{3/2} \rightarrow 4s \text{ } ^2\text{D}_{3/2}$	319.4	44544	13245
26	4p' $^2\text{P}_{3/2} \rightarrow 4s \text{ } ^2\text{D}_{3/2}$	306.3	45879	13245
27	4p' $^2\text{D}_{3/2} \rightarrow 4s \text{ } ^2\text{D}_{3/2}$	303.6	46173	13245

^a 1 eV = 8068 cm^{-1} .

1. Time-dependence of Ar and Cu atomic lines in a 10 μs -pulsed GD

Fig. 2 illustrates the characteristic time-dependent GD emission profiles at 10 μs pulse width, with argon transitions shown in (a) (750.4 nm ($2p_1-4p'[1/2] \rightarrow 1s_2-4s'[1/2]$), 772.4 nm ($2p_2-4p'[1/2] \rightarrow 1s_3-4s'[1/2]$), 415.9 nm ($3p_6-5p[3/2] \rightarrow 1s_5-4s[3/2]$), and 419.1 nm ($3p_4-5p'[3/2] \rightarrow 1s_3-4s'[1/2]$ and $3p_8-5p[5/2] \rightarrow 1s_5-4s[3/2]$)), together with copper transitions shown in (b) (327.4 nm ($4p \text{ } ^2\text{P}_{1/2} \rightarrow 4s \text{ } ^2\text{S}_{1/2}$), 303.6 nm ($4p' \text{ } ^2\text{D}_{3/2} \rightarrow 4s^2 \text{ } ^2\text{D}_{3/2}$), 221.5 nm ($4p' \text{ } ^2\text{P}_{3/2} \rightarrow 4s^2 \text{ } ^2\text{D}_{5/2}$), and 261.8 nm ($5p \text{ } ^2\text{P}_{3/2} \rightarrow 4s^2 \text{ } ^2\text{D}_{5/2}$)).

A significant emission peak is observed during the 10 μs pulse for each of the argon and copper neutral transitions, though their afterglow behavior varies significantly from line to line. The large initial peak after discharge initiation corresponds to the electron impact excitation. Free electrons are generated during the 10 μs electrical discharge and undergo several collisions with the particles in the plasma. Ground state argon atoms and sputtered copper atoms are thus excited to high energy levels followed with the spontaneous radiative relaxation. For argon atoms, the radiative decay of the transition $4p \rightarrow 4s$ and $5p \rightarrow 4s$ contributes the greatest part of UV-Vis Ar I emission spectra, which mainly forms the metastable argon atoms.

Some transitions of Ar I and Cu I are characterized by an afterglow that continues well beyond the end of the applied voltage pulse. The afterpeak can be easily observed with enough intensity for the transitions originated from relatively high-lying energy levels, such as 415.9 nm and 419.1 nm for argon, and 221.5 nm and 261.8 nm for copper. The relative intensity between the initial peak and afterpeak varies from line to line. For Cu I 221.5 nm, the afterpeak is even higher than the initial peak. This variation in the relative population of excited states during the pulse and afterglow regions indicates that the primary excitation mechanism differs during these two periods. The afterpeak is indicative of a recombination process, and the three-body recombination with an electron as its third body is primarily thought to be the dominant mechanism, although no specific mechanism has been assigned with certainty. During the excitation processes study on an rf-boostered pulsed Cu–Ne hollow cathode lamp, Farnsworth⁷ pointed out that the intensity of the afterglow, relative to that of a 10 μs current pulse and rf burst, rises with the energy of the upper state of the transition. Jackson and King⁵¹ measured the emitting species in the afterglow and also found the same phenomenon. All of these suggest that the cascade contribution from highly excited states is indeed largely responsible for the afterpeak.

The time gap between the initial peak and the afterglow may represent the initial rapid cooling of the electrons through collisions and the time required for speed electrons decelerating to allow recombination. As the electrons lose energy in inelastic collisions, conditions become favorable for recombination²⁰ and the afterglow intensity rises. The afterglow has been discussed by Falk and Lucht⁵² for a hollow cathode discharge, where decay times of $\tau = 18 \mu\text{s}$ and $7 \mu\text{s}$ were found for helium and argon discharge gas, respectively. Biondi and Brown²² reported that after discharge termination, the electron energies were thermalized in less than 50 μs , and Li⁵³ also found that $\sim 25 \mu\text{s}$ electron thermalization time was needed for recombination, which is in agreement with our results (25–35 μs time from initial peak to afterglow).

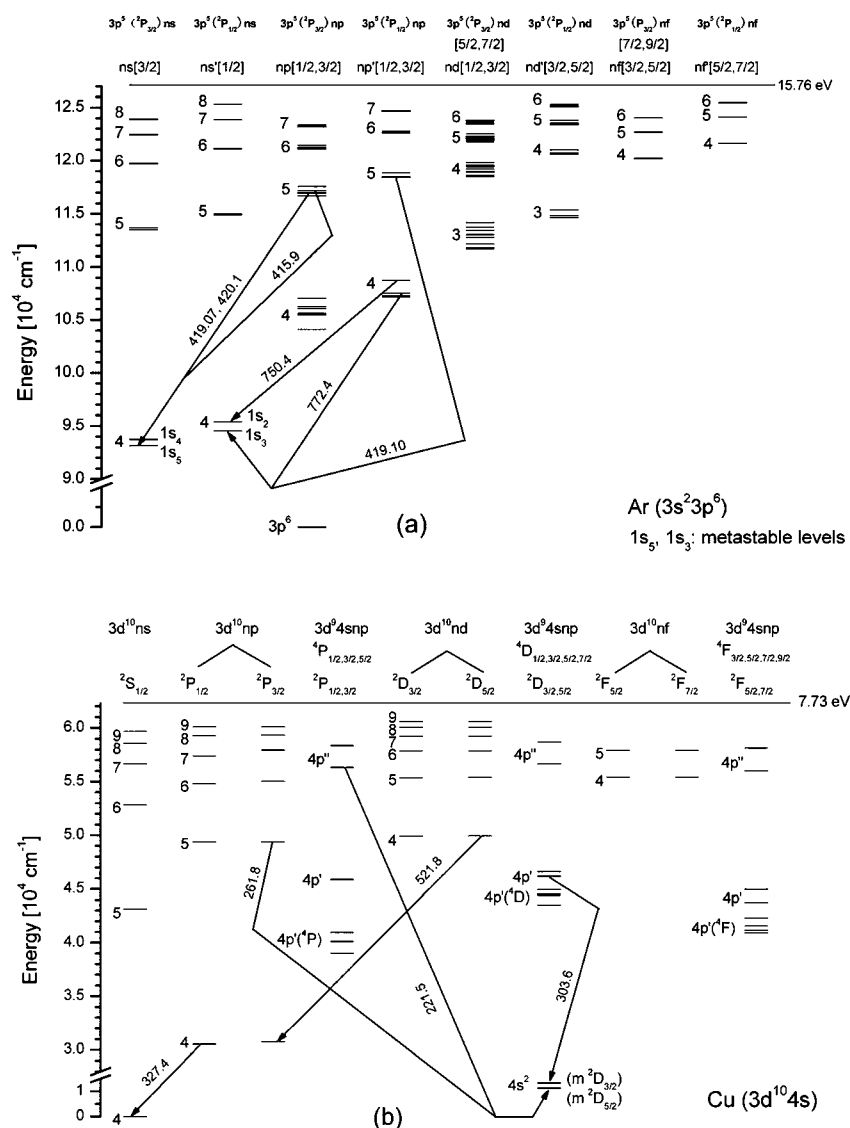


Fig. 1 Partial energy level diagrams for (a) argon and (b) copper.

Temporal profiles have been examined for those argon and copper neutral emission lines with intensities high enough to be recorded with our system. We found those as general rules: for argon, any transition from $5p \rightarrow 4s$ level has more evident afterpeak than that from $4p \rightarrow 4s$ level; and for copper, any radiative deexcitation from energy levels above 6 eV (higher than $4p'$ level, $1 \text{ eV} = 8068 \text{ cm}^{-1}$) has a distinguishable afterpeak. This rule is clearly demonstrated with the different temporal shapes for the 303.6 nm and 261.8 nm signals, for which there is only a little difference between their upper energy levels (see Table 2), but afterpeak can only be observed with 261.8 nm. In Ref. 35, Lewis *et al.* also revealed a distinct jump between electronic states of 5.78 eV and 6.12 eV in the calculated ratio of afterpeak-to-plateau. They explained that the jump was due to the electron excitation temperature during the discharge which had a mean value $\sim 6 \text{ eV}$. This would limit the population of levels above 6 eV during the discharge pulse region by electron excitation and lead to an increase in the calculated ratio. This explanation may not

be adequate, but there is almost no other reference explaining the phenomena.

Another feature of Fig. 2 is that the afterpeaks of argon and copper lines tend to appear at generally similar times after the pulse and then follow an exponential decay with time. Along with the trapping of the free electrons into the bound state of ions *via* recombination, the electron density decreases, as reflected in the decay of the afterpeak. The fact that sputtered copper exhibits afterpeaks with similar behavior as those of argon suggests that a similar process must be operative for both of them. The emission from the Cu I lines is more prolonged than the emission from the Ar I lines. This can be due to the formation of metastable argon atom accumulated during the plasma-on regime and in the afterglow, thus the continual formation of copper ions by Penning ionization occurs.⁵⁴ The afterpeaks are also relatively broader than the initial peaks and decay more slowly, which again indicates different excitation mechanisms for initial and post-pulse regions.

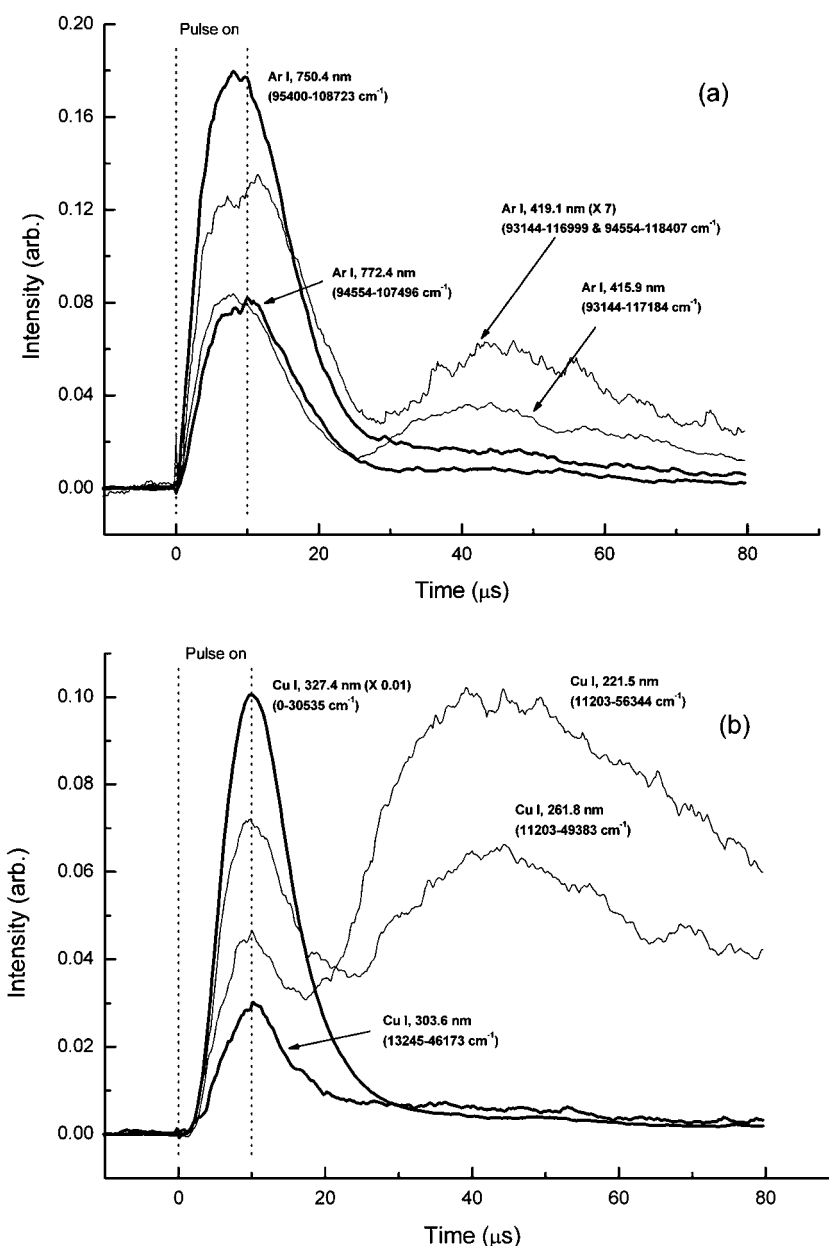


Fig. 2 Time dependent emission in a 10 μs -pulsed GD, (a) Ar I and (b) Cu I.

2. Time-dependence of Ar and Cu atomic lines in a 200 μs -pulsed GD

Additional temporal behavior study has been conducted at longer pulse regimes by extending the GD pulse width to 200 μs , providing additional pulse lifetime to generate plasma species. Argon lines shown in Fig. 3(a) and copper lines in 3(b) behave differently in the pulse and post-pulse time regimes.

During the discharge. These profiles show a large increase at the beginning of voltage pulse. Their peak shape and peak time resemble the initial peaks in Fig. 2, except for an intensity decrease here of about 10%, most likely from an inability of the power supply to sustain fully the extended pulse demand. Following the discharge pulse leading edge, the profiles then

manifest a quasi-stationary regime till 200 μs , the termination of the discharge. During the pulse-on period, Fig. 3(a) shows that for the argon 4p lines (750.4 nm and 772.4 nm); radiation decays slowly during the pseudo-stationary period; for 5p lines (419.1 nm and 415.9 nm), a similar slow decay is observed but with a small increase after 100 μs .

Time dependent phenomena for Cu emission are shown in Fig. 3(b). An evident difference in temporal behavior exists between copper lines originating from two upper energy level groupings (previously discussed). The transitions involving upper levels below 6 eV (324.7 nm and 303.6 nm) maintain a stable signal from the end of the initial peak to the termination of the GD pulse with the intensity of 20% of their first peak values. On the other hand, for the transitions originating from

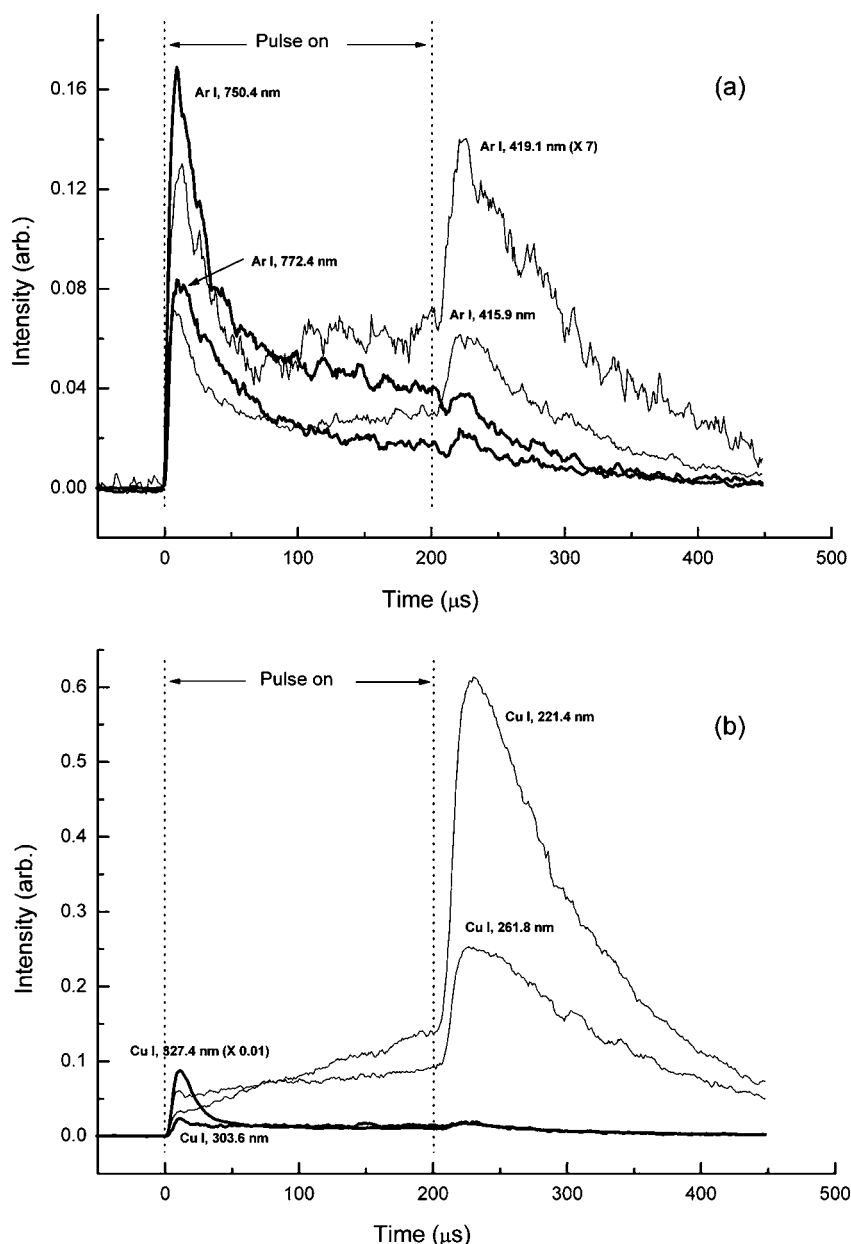


Fig. 3 Time dependent emission in a 200 μs-pulsed GD, (a) Ar I and (b) Cu I.

higher energy levels (221.4 nm and 261.8 nm), the gap between the initial peak and the pseudo-stationary regime is almost negligible, and the signal maintains a continuous increase during the pulse-on region.

For the excitation of plasma gas and sputtered atoms, the following processes must be the possible processes: electron impact excitation, metastable atoms (Penning) excitation, and recombination. Firstly, during the pulse-on region, electron temperature is so high that recombination reaction can be neglected; secondly, the behavior of argon lines can not be explained by Penning excitation mechanism, since argon metastable states of $1s_3$ and $1s_5$ are two of four terminating levels of argon $4p \rightarrow 4s$ or $5p \rightarrow 4s$ transitions; however, the copper atoms could be excited *via* penning excitation. Electron impact excitation may most likely be the primary excitation mechanism

for both argon and copper atoms. The electron temperature is increasing in this period due to electric power continuously deposited on the plasma. Along with the increasing electron energy, atoms are firstly excited, and then ionized. As a result, the fast decay of the initial peak of Cu I and Ar I lines during this region observed in Fig. 3 can be predicted due to the higher ionization fraction. As other evidence, a continuous increase of Cu(II) emission signal during the pulse-on region has been previously observed,³⁸ indicating the continuously increasing ionization rate.

Post discharge regime. In Fig. 3, following the end of the discharge pulse there is a sudden, substantial emission increase for some of the Cu I and Ar I lines with maxima located 25–35 μs after the pulse switched off. This time delay is almost the same

with either the 10 μs -pulse or the 200 μs -pulse, reflecting the same relaxation time required for the electrons to be thermalized and undergo recombination regardless of the pulse width. In Fig. 3(b), compared with the initial peak, the afterglow not only shows a strong intensity (4 or 20 times higher than their initial peak for Cu I 261.8 nm or Cu I 221.4 nm, respectively), but also a much broader profile. For those transitions originating from low-lying excited levels, the afterpeaks, which could not be observed in 10 μs -pulse, show only a small peak in 200 μs -pulse.

3. Effect of pulse width on recombination

As discussed previously, for both Ar I and Cu I lines, the intensity ratio between the afterpeak and the initial peak is much higher for the 200 μs -pulse compared with that of the 10 μs -pulse. To gain more detailed information on this phenomenon, the effect of pulse width on recombination processes was studied *via* observing the temporal behavior of various lines at different pulse widths (2, 5, 10, 20, 40, 80, 100, 200 μs). The power supply voltage output voltage was maintained constant in this experiment. Fig. 4 shows the time-dependent emission profiles of (a) Ar I 420.1 nm ($3p_9-5p[5/2] \rightarrow 1s_5-4s[3/2]$) and (b) Cu I 521.8 nm ($4d^2D_{5/2} \rightarrow 4p^2P_{3/2}$), respectively.

In Fig. 4(a), although the initial peak for Ar 420.1 nm broadens as the pulse width increases, the peak height varies a little. The afterpeak appeared even at very short pulse widths, suggesting that the densities of ions and electrons generated during a 2 μs -pulse GD are sufficient for the recombination process. The ratio of the afterpeak to the initial peak increases with the pulse width from 0.4 at 2 μs to 1.1 at 200 μs . For Cu I 521.8 nm in Fig. 4(b), this ratio maintains almost linear

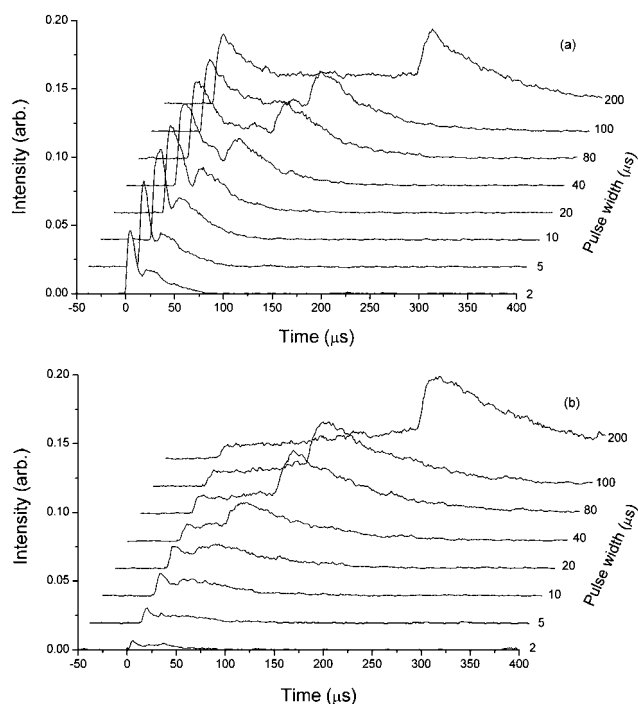


Fig. 4 Dependence of temporal emission profiles on the pulse width for (a) argon anomalous 420.1 nm line and (b) copper anomalous 521.8 nm line.

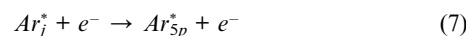
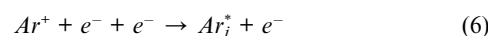
proportion to the pulse width: the value changed from 0.5 at 2 μs to 6.8 at 200 μs . This phenomenon can be explained by the accumulation of ions and electrons during the pulse-on regime, which enhances the recombination process at the plasma decay.

4. Three-body recombination process

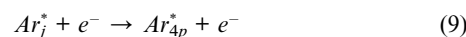
Afterglow can only be observed with certain argon and copper spectral lines. These lines involve the transition from relatively high energy levels, *e.g.* 5p level for argon or above 6 eV for copper. The relatively large excited state population in the early afterglow of the microsecond pulsed GD is ascribed to the three-body recombination process, especially for longer pulse widths.

In the afterglow, when the applied electric field suddenly disappears, the electrons will lose their kinetic energy in various collisions with the plasma particles. As the average velocity of the electrons decreases, the rate of the electron recombination with positive ions (argon ions or copper ions) will rise. After a free electron has been trapped and transferred to an energy state E_n in an ion through a three body collision (see eqn (5)), the excited atom may either be re-ionized (the opposite direction of this recombination) through electron impact or transferred to another bound state, through superelastic collisions with electrons or by radiative decay. In principle, the rate of recombination is a function of electron temperature and density, and may be calculated by solving a number of equations which express the population at the levels, N_n , and the various collision and radiative transition probabilities. For ionized hydrogen gas, at an electron temperature of 1000 K and electron densities $10^{12}\sim 10^{13}$ cm^{-3} , the calculated maximum contribution to the recombination rate comes from states with principal quantum number $n = 5, 6, 7, 8$.²⁹ For smaller n , the rate of collisional captures decreases, because larger energy exchanges are required in the two electron collision. For higher n , the re-ejection of the captured electron into the continuum becomes more and more probable. McWhirter²⁸ indicated that the three-body recombination rate (derived from the classic ionization rate) is proportional to the fourth power of the principal quantum number of the state into which the electron falls.

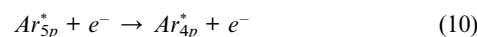
For a millisecond pulsed Grimm-type glow discharge, Human *et al.*⁶ described the three-body recombination process as following:



The energy level j usually lies near the ionization limit. The 5p-level can be reached through various cascades of the electron between higher levels, the final stage being the transition $5p \rightarrow 4s$, showing the intense afterpeak. Meanwhile, the 4p-level can also be reached *via* the same route as the 5p-level:



or



Since the recombination electron bound state decay is a downward process, that the population of 5p-level is higher than 4p-level leads to a strong afterglow for the transition involving jumps from 5p-levels. Similar afterpeak appearance time-delay for both Ar I and Cu I transitions indicates the same mechanism can also be applied for the copper afterglow emissions. However, we argue their explanation about the slow decaying emission tail of sputtered metal atoms in the afterglow.⁶ It is thought that the high energy electrons created *via* collisions of pairs of metastable argon atoms ($\text{Ar}_{4s} + \text{Ar}_{4s} \rightarrow \text{Ar}_{\text{ground}}^0 + \text{Ar}^+ + e^- + \Delta E$) excited the sputtered metal atom. Though the electron released in this process gains the difference in energy between the metastable levels and the ionization limit to have a kinetic energy between 7.2 and 7.9 eV, which is efficient to excite a copper atom, the different behavior of two groups of copper lines can not be elucidated. A downward population process, such as three-body recombination, is more reasonable to be ascribed to. The energy flow of the downward process arises from the plasma decay after the discharge pulsed is terminated. The argon ion–electron–electron recombination-decay forms argon metastable atoms and the plasma energy cascades from the argon ion to the argon metastable state. Then Penning ionization of copper atom transfers the energy of argon metastable atoms to the copper ion. Finally the copper ion three-body recombination causes the energy cascading to the excited copper atom. Thus, High lying excited levels can be more densely settled rather than low lying energy levels.

Conclusion

The glow discharge comprises complex processes. The relative importance of each mechanism varies depending on the discharge operation conditions. Three-body recombination occurs more readily in a high pressure, high current GD than in a low pressure, low current GD. In a low pressure, low current source, the electron density is low. The mean free path for the electron could be in sub-millimetre or millimetre range, which facilitates high energy electron diffusion from the analytical negative glow region. Thus, the percentage of the electrons involving the three-body combination process could be reduced. But for a GD emission source, where high pressure and high current are preferred, the collisional-radiative recombination process will become significant.

The data presented here suggest the following excitation processes for Cu and Ar neutral spectra in the microsecond pulsed glow discharge. During the applied voltage pulse, electron impact excites the neutral spectrum. The afterglow arises from a three-body recombination. The longer the pulse width, the higher the afterpeak observed. For both the discharge gas and analyte transitions, two categories can be considered. A general rule is found that lines from low energy level have small afterpeaks, while lines from high energy level show intense afterpeaks. The upper energy level is a crucial factor in determining the afterpeak intensity through a three-body recombination process. However, the reason why upper energy level of 6 eV for copper is the turning point of the afterpeak is still not fully understood.

Dissociative recombination, which was suggested to be the determining mechanism for millisecond pulsed discharges⁸ is probably excluded as the main mechanism for the afterglow in μs

GD, based on the low Ar_2^+ signal in the mass spectrum, which reflects its overall low density. However, depending on the position of the ion formation, there exists a time delay of several microseconds between the ion formation and being sampled into MS. It is unknown whether the Ar_2^+ density changes dramatically in the time delay; therefore, dissociative recombination cannot yet completely be ruled out for a microsecond pulsed discharge. A more detailed study is necessary for a clearer depiction of the afterglow mechanism for microsecond pulsed GD.

Acknowledgements

This work was supported by grants from the Department of Energy, Basic Energy Sciences, and National Natural Science Foundation of China, for which we are most grateful.

References

- 1 W. W. Harrison, K. R. Hess, R. K. Marcus and F. L. King, *Anal. Chem.*, 1986, **58**, 341A.
- 2 R. K. Marcus, *Glow Discharge Spectroscopies*, Plenum Press, New York, 1993.
- 3 P. Šmid, E. Steers, Z. Weiss, J. Pickering and V. Hoffmann, *J. Anal. At. Spectrom.*, 2008, **23**, 1223.
- 4 A. Bogaerts, E. Wagner, B. W. Smith, J. D. Winefordner, D. Pollmann, W. W. Harrison and R. Gijbels, *Spectrochim. Acta, Part B*, 1997, **52B**, 205.
- 5 N. P. Ferreira, J. A. Strauss and H. G. C. Human, *Spectrochim. Acta, Part B*, 1983, **38B**, 899.
- 6 J. A. Strauss, N. P. Ferreira and H. G. C. Human, *Spectrochim. Acta, Part B*, 1982, **37B**, 947.
- 7 P. B. Farnsworth and J. P. Walters, *Spectrochim. Acta, Part B*, 1982, **37B**, 773.
- 8 A. Bogaerts, *J. Anal. At. Spectrom.*, 2007, **22**, 502.
- 9 A. Bogaerts, R. Gijbels and G. P. Jackson, *J. Anal. At. Spectrom.*, 2003, **18**, 533.
- 10 A. Bogaerts and R. Gijbels, *J. Anal. At. Spectrom.*, 2001, **16**, 239.
- 11 W. Hang, C. Baker, B. W. Smith, J. D. Winefordner and W. W. Harrison, *J. Anal. At. Spectrom.*, 1997, **12**, 143.
- 12 E. Oxley, C. L. Yang, J. Liu and W. W. Harrison, *Anal. Chem.*, 2003, **75**, 6478.
- 13 E. Oxley, K. Turney, J. Gasser and W. W. Harrison, *J. Anal. At. Spectrom.*, 2003, **18**, 1376.
- 14 W. W. Harrison, W. Hang, X. M. Yan, K. Ingeneri and C. Schilling, *J. Anal. At. Spectrom.*, 1997, **12**, 891.
- 15 C. L. Lewis, M. A. Moser, W. Hang, D. E. Dale, D. C. Hassell and V. Majidi, *J. Anal. At. Spectrom.*, 2003, **18**, 629.
- 16 W. W. Harrison and W. Hang, *Fresenius J. Anal. Chem.*, 1996, **355**, 803.
- 17 M. R. Winchester and R. K. Marcus, *Anal. Chem.*, 1992, **64**, 2067.
- 18 J. A. Klingler, C. M. Barshick and W. W. Harrison, *Anal. Chem.*, 1991, **63**, 2571.
- 19 J. A. Klinger, P. J. Savickas and W. W. Harrison, *J. Am. Soc. Mass Spectrom.*, 1990, **1**, 138.
- 20 J. B. Hasted, 2nd edition, *Physics of Atomic Collisions*, American Elsevier Publishing Company, Inc. 1972, ch. 7.
- 21 D. Ohebsian, N. Sadeghi, C. Trassy and J. M. Mermet, *Opt. Commun.*, 1980, **32**, 81.
- 22 M. A. Biondi and S. C. Brown, *Phys. Rev.*, 1949, **76**, 1697.
- 23 M. A. Biondi and S. C. Brown, *Phys. Rev.*, 1949, **75**, 1700.
- 24 C. Kenty, *Phys. Rev.*, 1928, **32**, 624.
- 25 D. R. Bates, *Phys. Rev.*, 1950, **77**, 718.
- 26 D. R. Bates, *Phys. Rev.*, 1950, **78**, 492.
- 27 T. R. Connor and M. A. Biondi, *Phys. Rev.*, 1965, **140**, 778.
- 28 R. W. P. McWhirter, *Nature*, 1961, **190**, 902.
- 29 N. D'Angelo, *Phys. Rev.*, 1961, **121**, 505.
- 30 E. Hinnov and J. G. Hirschberg, *Phys. Rev.*, 1962, **125**, 795.
- 31 V. A. Kartazhev, Y. A. Piotrovskii and Y. A. Tolmachev, *Opt. Spektrosk.*, 1977, **42**, 1048.

- 32 Y. M. Kagan, N. B. Kolokolov and P. M. Pramatarov, *Opt. Spektrosk.*, 1977, **42**, 252.
- 33 F. E. Irons and N. J. Peacock, *J. Phys. B: At. Mol. Phys.*, 1974, **7**, 2084.
- 34 G. P. Jackson, C. L. Lewis, S. K. Doorn, V. Majidi and F. L. King, *Spectrochim. Acta, Part B*, 2001, **56**, 2449.
- 35 C. L. Lewis, G. P. Jackson, S. K. Doorn, V. Majidi and F. L. King, *Spectrochim. Acta, Part B*, 2001, **56**, 487.
- 36 G. Gamez, A. Bogaerts and G. M. Hieftje, *J. Anal. At. Spectrom.*, 2006, **21**, 350.
- 37 A. Bogaerts and R. Gijbels, *J. Anal. At. Spectrom.*, 2000, **15**, 895.
- 38 X. Yan, K. Ingeneri, W. Hang and W. W. Harrison, *J. Anal. At. Spectrom.*, 2001, **16**, 819.
- 39 L. B. Loeb, *Basic Processes of Gaseous Electronic*, University of California Press, Berkeley and Los Angeles, 1955, ch. VI.
- 40 R. B. Holt, J. M. Richardson, B. Howland and B. T. McClure, *Phys. Rev.*, 1950, **77**, 239.
- 41 N. P. Ferreira, H. G. C. Human and L. R. P. Butler, *Spectrochim. Acta Part B*, 1980, **35B**, 287.
- 42 D. Fang and R. K. Marcus, *Spectrochim. Acta, Part B*, 1991, **46B**, 983.
- 43 R. Hugon, G. Henrion and M. Fabry, *Plasma Sources Sci. Technol.*, 1996, **5**, 553.
- 44 A. Martin, N. Bordel, R. Pereiro and A. Bogaerts, *Spectrochim. Acta, Part B*, 2008, **63**, 1274.
- 45 F. L. King and C. Pan, *Anal. Chem.*, 1993, **65**, 735.
- 46 M. A. Biondi, *Phys. Rev.*, 1963, **129**, 1181.
- 47 A. Al-Jalal and M. A. Khan, *J. Appl. Phys.*, 2006, **99**, 033302–1.
- 48 Y. Hahn, *Phys. Lett. A*, 1997, **231**, 82.
- 49 C. E. Moore, *Atomic Energy Levels, Vol. II (Chromium through Niobium)*, Circular of the National Bureau of Standards 467, U.S. Government Printing Office, Washington, DC. 1952.
- 50 C. E. Moore, *Atomic Energy Levels, Vol. I (Hydrogen through Vanadium)*, Circular of the National Bureau of Standards 467, U.S. Government Printing Office, Washington, DC. 1949.
- 51 G. P. Jackson and F. L. King, *Spectrochim. Acta, Part B*, 2003, **58**, 1417.
- 52 H. Falk and H. Lucht, *J. Quant. Spectrosc. Radiat. Transfer*, 1976, **16**, 909.
- 53 L. Li, J. Robertson-Honecker, V. Vaghela and F. L. King, *Spectrochim. Acta, Part B*, 2006, **61**, 722.
- 54 G. P. Jackson and F. L. King, *Spectrochim. Acta, Part B*, 2003, **58**, 185.